

Semileptonic and radiative decays of the B_c meson in light-front quark model

Ho-Meoyng Choi^a and Chueng-Ryong Ji^b

^a Department of Physics, Teachers College, Kyungpook National University, Daegu, Korea 702-701

^b Department of Physics, North Carolina State University, Raleigh, NC 27695-8202

We investigate the exclusive semileptonic $B_c \rightarrow (D, \eta_c, B, B_s)\ell\nu_\ell$, $\eta_b \rightarrow B_c\ell\nu_\ell$ ($\ell = e, \mu, \tau$) decays using the light-front quark model constrained by the variational principle for the QCD motivated effective Hamiltonian. The form factor $f_+(q^2)$, which is free from the zero mode, can be obtained from the analytic continuation method in the $q^+ = 0$ frame. However, the form factor $f_-(q^2)$, which is not free from the zero mode in the $q^+ = 0$ frame, needs to be obtained in the $q^+ \neq 0$ frame with the effective treatment based on the Bethe-Salpeter formalism in handling the nonvalence (higher Fock states) contribution. We verify the covariance of our model calculation by checking the consistency between the two results of $f_+(q^2)$; one from the analytic continuation and the other from the effective treatment of handling the nonvalence contribution. Our results are then compared to the available experimental data and the results from other theoretical approaches. Since the prediction on the magnetic dipole $B_c^* \rightarrow B_c + \gamma$ decay turns out to be very sensitive to the mass difference between B_c^* and B_c mesons, our prediction both on the unmeasured B_c^* meson mass and the decay width $\Gamma(B_c^* \rightarrow B_c\gamma)$ may help in determining the mass of B_c^* experimentally.

I. INTRODUCTION

The exclusive semileptonic decay processes of heavy mesons generated a great excitement not only in extracting the most accurate values of Cabibbo-Kobayashi-Maskawa (CKM) matrix elements but also in testing diverse theoretical approaches to describe the internal structure of hadrons. The great virtue of semileptonic decay processes is that the effects of the strong interaction can be separated from the effects of the weak interaction into a set of Lorentz-invariant form factors, i.e., the essential informations of the strongly interacting quark/gluon structure inside hadrons. Thus, the theoretical problem associated with analyzing semileptonic decay processes is essentially that of calculating the weak form factors.

In particular, along with the experimental study planned both at the Tevatron and at the Large Hadron Collider (LHC), the study of the B_c meson has been very interesting due to its outstanding feature; i.e., the B_c meson is the lowest bound state of two heavy (b, c) quarks with different flavors. Because of the fact that the B_c meson carries the flavor explicitly, not like the symmetric heavy quarkonium ($b\bar{b}$, $c\bar{c}$) states, there is no gluon or photon annihilation via strong interaction or electromagnetic interaction. It can decay only via weak interaction. Since both b - and c -quarks forming the B_c meson are heavy, the B_c meson can decay appreciably not only through the $b \rightarrow q$ ($q = c, u$) transition with c quark being a spectator but also through the $c \rightarrow q$ ($q = s, d$) transition with b quark being a spectator. The former transitions correspond to the semileptonic decays to η_c and D mesons, while the latter transitions correspond to the decays to B_s and B mesons. The latter transitions are governed typically by much larger CKM matrix element; e.g., $|V_{cs}| \sim 1$ for $B_c \rightarrow B_s\ell\nu_\ell$ ($\ell = e, \mu$), vs. $|V_{cb}| \sim 0.04$ for $B_c \rightarrow \eta_c\ell\nu_\ell$ ($\ell = e, \mu, \tau$). Although the phase space in $c \rightarrow s, d$ transitions is much smaller than that in $b \rightarrow c, u$ transitions, the c -quark decays provide about $\sim 70\%$ to

the decay width of B_c . The b -quark decays and weak annihilation add about 20 and 10%, respectively [1]. This indicates that both b - and c -quark decay processes contribute on a comparable footing to the B_c decay width.

There are many theoretical approaches to the calculation of exclusive B_c semileptonic decay modes. Although we may not be able to list them all, we may note here the following works: QCD sum rules [1, 2, 3, 4], the relativistic quark model [5, 6, 7] based on an effective Lagrangian describing the coupling of hadrons to their constituent quarks, the quasipotential approach to the relativistic quark model [8, 9, 10], the instantaneous nonrelativistic approach to the Bethe-Salpeter (BS) equation [11], the relativistic quark model based on the BS equation [12, 13], the QCD relativistic potential model [14], the relativistic quark-meson model [15], the nonrelativistic quark model [16], the covariant light-front quark model [17], and the constituent quark model [18, 19, 20, 21] using BSW (Bauer, Stech, and Wirbel) model [22] and ISGW (Isgur, Scora, Grinstein, and Wise) model [23].

The purpose of this paper is to calculate the hadronic form factors and decay widths for the exclusive semileptonic $B_c \rightarrow P\ell\nu_\ell$ ($P = D, D_s, B, B_s$) and $\eta_b \rightarrow B_c\ell\nu_\ell$ decays and the magnetic dipole $B_c^* \rightarrow B_c\gamma$ transition using our light-front quark model (LFQM) [24, 25, 26, 27, 28, 29] based on the QCD-motivated effective LF Hamiltonian. In our previous LFQM analysis [24, 25, 26, 27, 28, 29], we have analyzed the mass spectra and various exclusive processes of the ground state pseudoscalar (P) and vector (V) mesons except B_c and B_c^* mesons. We have analyzed, for example, the meson mass spectra [24, 25], the $P \rightarrow P$ semileptonic heavy/light meson decays [25, 26], the rare $B \rightarrow K\ell^+\ell^-$ decays [27], and the magnetic dipole transitions between the low-lying heavy/light pseudoscalar/vector mesons [24, 28, 29]. In those analyses, we found a good agreement with the experimental data. In this work, we extend our LFQM to predict the masses and the decay

constants of B_c and B_c^* mesons as well as the above mentioned exclusive decays of B_c and B_c^* mesons.

Our LFQM [24, 25, 26, 27, 28, 29] analysis in this work has several salient features: (1) We have implemented the variational principle to the QCD motivated effective LF Hamiltonian to enable us to analyze the meson mass spectra and to find optimized model parameters. The present investigation further constrains the phenomenological parameters and extends the applicability of our LFQM to the wider range of hadronic phenomena. (2) We have performed the analytical continuation from the spacelike region to the physical timelike region to obtain the weak form factor $f_+(q^2)$ for the exclusive semileptonic decays between the two pseudoscalar mesons as well as to obtain the decay form factors $F_{VP}(q^2)$ for $V \rightarrow P\gamma^*$ transitions. The Drell-Yan-West($q^+ = q^0 + q^3 = 0$) frame is useful because only the valence contributions are needed when the “+” component of the currents is used. (3) We have developed an effective treatment of handling the higher Fock state(or nonvalence) contribution to the weak form factor $f_-(q^2)$, which is known to receive higher Fock state contributions(e.g., zero mode in the $q^+ = 0$ frame or nonvalence contribution in the $q^+ \neq 0$ frame) within the framework of LF quantization. Thus, we utilize both the analytic method in the $q^+ = 0$ frame to obtain (f_+ , $F_{B_c^*B_c}$) and the effective method in the $q^+ > 0$ frame to obtain f_- , respectively.

The paper is organized as follows. In Sec. II, we briefly describe the formulation of our LFQM and the procedure of fixing the model parameters using the variational principle for the QCD motivated effective Hamiltonian. The masses and decay constants of the B_c^* and B_c mesons are predicted and compared with the data as well as other theoretical model predictions. The distribution amplitudes(DAs) for the heavy-flavored mesons such as D, η_c, B, B_s, B_c and η_b are also obtained in this section. In Sec. III, we calculate the weak form factors $f_+(q^2)$ and $f_-(q^2)$ using our LFQM. To obtain $f_+(q^2)$, we use the $q^+ = 0$ frame(i.e., $q^2 = -\mathbf{q}_\perp^2 < 0$) and then analytically continue the results to the timelike $q^2 > 0$ region by changing \mathbf{q}_\perp^2 to $-q^2$ in the form factor. The form factor $f_-(q^2)$ is obtained from our effective method [26] in the purely longitudinal $q^+ > 0$ frame(i.e., $q^2 = q^+q^- > 0$). In Sec. IV, the decay form factor $F_{B_c^*B_c}(q^2)$ for the $B_c^* \rightarrow B_c\gamma^*$ transition and the decay width for $B_c^* \rightarrow B_c\gamma$ are presented. Again the form factor $F_{B_c^*B_c}(q^2)$ is obtained the $q^+ = 0$ frame and then analytically continued to the timelike region. The coupling constant $g_{B_c^*B_c}$ needed for the calculation of the decay width for $B_c^* \rightarrow B_c\gamma$ is determined in the limit $q^2 \rightarrow 0$, i.e., $g_{B_c^*B_c} = F_{B_c^*B_c}(q^2 = 0)$. In Sec. V, our numerical results (i.e., the form factors and decay rates for $B_c \rightarrow (D, \eta_c, B, B_s)\ell\nu_\ell$, $\eta_b \rightarrow B_c\ell\nu_\ell$, and $B_c^* \rightarrow B_c\gamma^{(*)}$ decays) are presented and compared with the experimental data as well as other theoretical results. Summary and discussion follow in Sec.VI.

II. MODEL DESCRIPTION

The key idea in our LFQM [24, 25] for mesons is to treat the radial wave function as a trial function for the variational principle to the QCD-motivated effective Hamiltonian saturating the Fock state expansion by the constituent quark and antiquark. The QCD-motivated Hamiltonian for a description of the ground state meson mass spectra is given by

$$\begin{aligned} H_{q\bar{q}}|\Psi_{nlm}^{JJ_z}\rangle &= \left[\sqrt{m_q^2 + \vec{k}^2} + \sqrt{m_{\bar{q}}^2 + \vec{k}^2} + V_{q\bar{q}} \right] |\Psi_{nlm}^{JJ_z}\rangle, \\ &= [H_0 + V_{q\bar{q}}]|\Psi_{nlm}^{JJ_z}\rangle = M_{q\bar{q}}|\Psi_{nlm}^{JJ_z}\rangle, \end{aligned} \quad (1)$$

where $\vec{k} = (\mathbf{k}_\perp, k_z)$ is the three-momentum of the constituent quark, $M_{q\bar{q}}$ is the mass of the meson, and $|\Psi_{nlm}^{JJ_z}\rangle$ is the meson wave function. In this work, we use two interaction potentials $V_{q\bar{q}}$; (1) Coulomb plus harmonic oscillator(HO) and (2) Coulomb plus linear confining potentials. The hyperfine interaction essential to distinguish pseudoscalar(0^{-+}) and vector(1^{--}) mesons is also included; viz.,

$$V_{q\bar{q}} = V_0 + V_{\text{hyp}} = a + \mathcal{V}_{\text{conf}} - \frac{4\alpha_s}{3r} + \frac{2}{3} \frac{\mathbf{S}_q \cdot \mathbf{S}_{\bar{q}}}{m_q m_{\bar{q}}} \nabla^2 V_{\text{coul}}, \quad (2)$$

where $\mathcal{V}_{\text{conf}} = br(r^2)$ for the linear (HO) potential and $\langle \mathbf{S}_q \cdot \mathbf{S}_{\bar{q}} \rangle = 1/4(-3/4)$ for the vector (pseudoscalar) meson. Using this Hamiltonian, we analyze the meson mass spectra and various wave-function-related observables, such as decay constants, electromagnetic form factors of mesons in a spacelike region, and the weak form factors for the exclusive semileptonic and rare decays of pseudoscalar mesons in the timelike region [24, 25, 26, 27, 28, 29].

The momentum-space light-front wave function of the ground state pseudoscalar and vector mesons is given by

$$\Psi_{100}^{JJ_z}(x_i, \mathbf{k}_{i\perp}, \lambda_i) = \mathcal{R}_{\lambda_1\lambda_2}^{JJ_z}(x_i, \mathbf{k}_{i\perp})\phi(x_i, \mathbf{k}_{i\perp}), \quad (3)$$

where $\phi(x_i, \mathbf{k}_{i\perp})$ is the radial wave function and $\mathcal{R}_{\lambda_1\lambda_2}^{JJ_z}$ is the spin-orbit wave function that is obtained by the interaction-independent Melosh transformation from the ordinary spin-orbit wave function assigned by the quantum numbers J^{PC} . The model wave function in Eq. (3) is represented by the Lorentz-invariant internal variables, $x_i = p_i^+/P^+$, $\mathbf{k}_{i\perp} = \mathbf{p}_{i\perp} - x_i\mathbf{P}_\perp$ and λ_i , where $P^\mu = (P^+, P^-, \mathbf{P}_\perp) = (P^0 + P^3, (M^2 + \mathbf{P}_\perp^2)/P^+, \mathbf{P}_\perp)$ is the momentum of the meson M , and p_i^μ and λ_i are the momenta and the helicities of constituent quarks, respectively.

The covariant forms of the spin-orbit wave functions for pseudoscalar and vector mesons are given by

$$\begin{aligned} \mathcal{R}_{\lambda_1\lambda_2}^{00} &= \frac{-\bar{u}(p_1, \lambda_1)\gamma_5 v(p_2, \lambda_2)}{\sqrt{2}\tilde{M}_0}, \\ \mathcal{R}_{\lambda_1\lambda_2}^{1J_z} &= \frac{-\bar{u}(p_1, \lambda_1) \left[\not{\epsilon}(J_z) - \frac{\epsilon \cdot (p_1 - p_2)}{M_0 + m_1 + m_2} \right] v(p_2, \lambda_2)}{\sqrt{2}\tilde{M}_0}, \end{aligned} \quad (4)$$

where $\tilde{M}_0 = \sqrt{M_0^2 - (m_1 - m_2)^2}$, M_0^2 is the invariant meson mass square defined by $M_0^2 = \sum_{i=1}^2 \frac{\mathbf{k}_{i\perp}^2 + m_i^2}{x_i}$, and $\epsilon^\mu(J_z)$ is the polarization vector of the vector meson [30]. The spin-orbit wave functions satisfy the relation $\sum_{\lambda_1 \lambda_2} \mathcal{R}_{\lambda_1 \lambda_2}^{JJ_z \dagger} \mathcal{R}_{\lambda_1 \lambda_2}^{JJ_z} = 1$ for both pseudoscalar and vector mesons. For the radial wave function ϕ , we use the same Gaussian wave function for both pseudoscalar and vector mesons:

$$\phi(x_i, \mathbf{k}_{i\perp}) = \frac{4\pi^{3/4}}{\beta^{3/2}} \sqrt{\frac{\partial k_z}{\partial x}} \exp(-\vec{k}^2/2\beta^2), \quad (5)$$

where β is the variational parameter. When the longitudinal component k_z is defined by $k_z = (x - 1/2)M_0 + (m_2^2 - m_1^2)/2M_0$, the Jacobian of the variable transformation $\{x, \mathbf{k}_\perp\} \rightarrow \vec{k} = (\mathbf{k}_\perp, k_z)$ is given by

$$\frac{\partial k_z}{\partial x} = \frac{M_0}{4x_1 x_2} \left\{ 1 - \left[\frac{m_1^2 - m_2^2}{M_0^2} \right]^2 \right\}. \quad (6)$$

Note that the free kinetic part of the Hamiltonian $H_0 = \sqrt{m_q^2 + \vec{k}^2} + \sqrt{m_{\bar{q}}^2 + \vec{k}^2}$ is equal to the free mass operator M_0 in the light-front formalism.

The normalization factor in Eq. (5) is obtained from the following normalization of the total wave function:

$$\int_0^1 dx \int \frac{d^2 \mathbf{k}_\perp}{16\pi^3} |\Psi_{100}^{JJ_z}(x, \mathbf{k}_{i\perp})|^2 = 1. \quad (7)$$

We apply our variational principle to the QCD-motivated effective Hamiltonian first to evaluate the expectation value of the central Hamiltonian $H_0 + V_0$, *i.e.*, $\langle \phi | (H_0 + V_0) | \phi \rangle$ with a trial function $\phi(x_i, \mathbf{k}_{i\perp})$ that depends on the variational parameter β . Once the model parameters are fixed by minimizing the expectation value $\langle \phi | (H_0 + V_0) | \phi \rangle$, then the mass eigenvalue of each meson is obtained as $M_{q\bar{q}} = \langle \phi | (H_0 + V_{q\bar{q}}) | \phi \rangle$. Following the above procedure, we find an analytic form of the mass eigenvalue given by

$$M_{q\bar{q}} = \frac{1}{\beta\sqrt{\pi}} \sum_{i=q,\bar{q}} m_i^2 e^{m_i^2/2\beta^2} K_1\left(\frac{m_i^2}{2\beta^2}\right) + a \mathbf{1} + b \left(\frac{2}{\beta\sqrt{\pi}} \right) - \alpha_s \left[\frac{8\beta}{3\sqrt{\pi}} + \frac{32\beta^3 \langle \mathbf{S}_q \cdot \mathbf{S}_{\bar{q}} \rangle}{9m_q m_{\bar{q}} \sqrt{\pi}} \right] \mathbf{1}, \quad (8)$$

where $\mathbf{1} = \begin{pmatrix} 1 \\ 1 \end{pmatrix}$ and $K_1(x)$ is the modified Bessel function of the second kind. The upper and lower components of the column vector in Eq. (8) represent the results for the linear and HO potential models, respectively. Minimizing energies with respect to β and searching for a fit to the observed ground state meson spectra, our central potential V_0 obtained from our optimized potential parameters ($a = -0.72$ GeV, $b = 0.18$ GeV², and $\alpha_s = 0.31$) [24] for Coulomb plus linear potential was found to be quite

comparable with the quark potential model suggested by Scora and Isgur [31] where they obtained $a = -0.81$ GeV, $b = 0.18$ GeV², and $\alpha_s = 0.3 \sim 0.6$ for the Coulomb plus linear confining potential. A more detailed procedure for determining the model parameters of light- and heavy-quark sectors can be found in our previous works [24, 25]. In this work, we obtain the new variational parameter β_{cb} for the bottom-charm sector and predict the mass eigenvalues of the low-lying B_c and B_c^* states. Our new prediction of $M_{B_c} = 6459$ [6351] MeV obtained from the linear [HO] potential model is in agreement with the data, $M_{B_c}^{\text{exp}} = (6276 \pm 4)$ MeV [32] within 3% error. We also predict the unmeasured mass of B_c^* as $M_{B_c^*} = 6494$ [6496] MeV for the linear [HO] potential model.

Our model parameters ($m_q, \beta_{q\bar{q}}$) and the predictions of the ground state meson mass spectra obtained from the linear and HO potential models are summarized in Table I and in Fig. 1, respectively, compared with the experimental data [32]. Our prediction of the η_b meson obtained from the linear [HO] potential model, $M_{\eta_b} = 9657$ [9295] MeV slightly overestimates[underestimates] the very recent data from the Babar experiment, $M_{\eta_b}^{\text{exp}} = 9388.9_{-2.3}^{+3.1}(\text{stat}) \pm 2.7(\text{syst})$ MeV [33]. Overall, however, our LFQM predictions of the ground state meson mass spectra are in agreement with the data [32] within 6% error.

The decay constants of pseudoscalar and vector mesons are defined by

$$\begin{aligned} \langle 0 | \bar{q} \gamma^\mu \gamma_5 q | P \rangle &= i f_P P^\mu, \\ \langle 0 | \bar{q} \gamma^\mu q | V(P, h) \rangle &= f_V M_V \epsilon^\mu(h). \end{aligned} \quad (9)$$

In the above definitions for the decay constants, the experimental values of pion and rho meson decay constants are $f_\pi \approx 131$ MeV from $\pi \rightarrow \mu\nu$ and $f_\rho \approx 220$ MeV from $\rho \rightarrow e^+e^-$.

Using the plus component ($\mu = +$) of the currents, one can easily calculate the decay constants. The explicit forms of pseudoscalar and vector meson decay constants are given by

$$\begin{aligned} f_P &= 2\sqrt{6} \int \frac{dx d^2 \mathbf{k}_\perp}{16\pi^3} \frac{\mathcal{A}}{\sqrt{\mathcal{A}^2 + \mathbf{k}_\perp^2}} \phi(x, \mathbf{k}_\perp), \\ f_V &= 2\sqrt{6} \int \frac{dx d^2 \mathbf{k}_\perp}{16\pi^3} \frac{\phi(x, \mathbf{k}_\perp)}{\sqrt{\mathcal{A}^2 + \mathbf{k}_\perp^2}} \left[\mathcal{A} + \frac{2\mathbf{k}_\perp^2}{\mathcal{M}_0} \right], \end{aligned} \quad (10)$$

where $\mathcal{A} = x_2 m_1 + x_1 m_2$ and $\mathcal{M}_0 = M_0 + m_1 + m_2$. We note that the vector meson decay constant f_V is extracted from the longitudinal ($h = 0$) polarization.

In Table II, we present our predictions for the decay constants of f_{B_c} and $f_{B_c^*}$ and compare with other model calculations. The decay constants for other light- and heavy-mesons have been predicted in our previous works [28, 30].

The quark distribution amplitudes(DAs) for pseudoscalar (vector) mesons are constrained by

$$\int_0^1 \phi_{P(V)}(x) dx = \frac{f_{P(V)}}{2\sqrt{6}}. \quad (11)$$

TABLE I: The constituent quark mass [GeV] and the Gaussian parameters β [GeV] for the linear and HO potentials obtained by the variational principle. $q = u$ and d .

Model	m_q	m_s	m_c	m_b	β_{qq}	β_{qs}	β_{ss}	β_{qc}	β_{sc}	β_{cc}	β_{qb}	β_{sb}	β_{cb}	β_{bb}
Linear	0.22	0.45	1.8	5.2	0.3659	0.3886	0.4128	0.4679	0.5016	0.6509	0.5266	0.5712	0.8068	1.1452
HO	0.25	0.48	1.8	5.2	0.3194	0.3419	0.3681	0.4216	0.4686	0.6998	0.4960	0.5740	1.0350	1.8025

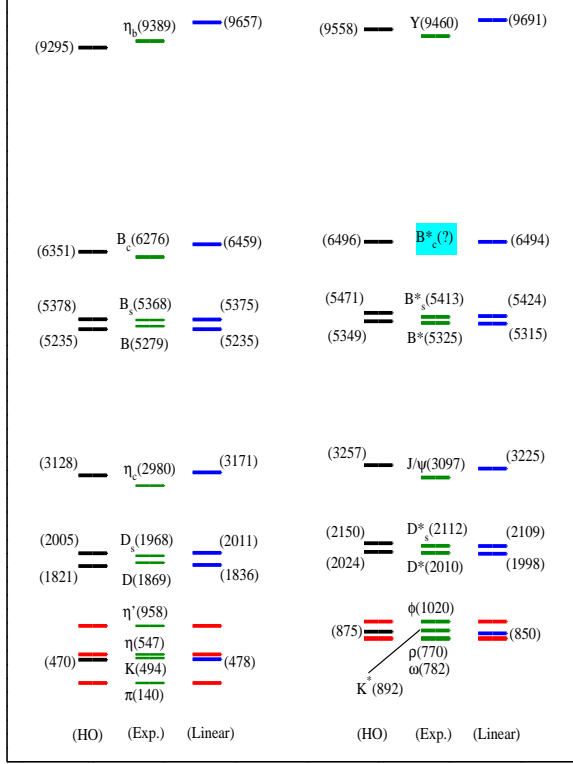


FIG. 1: (color online). Fit of the ground state meson masses [MeV] with the parameters given in Table I. The (ρ, π) , (η, η') , and (ω, ϕ) masses are our input data. The masses of $(\omega - \phi)$ and $(\eta - \eta')$ were used to determine the mixing angles of $\omega - \phi$ and $\eta - \eta'$ [24], respectively.

TABLE II: Bottom-charm meson decay constants (in unit of MeV) obtained from the linear [HO] parameters.

	Linear	[HO]	[5]	[8]	[34]	[35]	[36]	[37]
f_{B_c}	377	[508]	360	433	500	460 ± 60	517	410 ± 40
$f_{B_s^*}$	398	[551]	—	503	500	460 ± 60	517	—

We show in Fig. 2 the normalized quark DAs $\Phi(x) = (2\sqrt{6}/f_P)\phi(x)$ for D (dotted line), B (dashed line), B_s (dot-dashed line), and B_c (solid line) mesons obtained from the linear (upper panel) and HO (lower panel) potential parameters, respectively. In Fig. 3, we also show the normalized quark DAs for η_c (thin lines) and η_b (thick lines) mesons obtained from the linear (solid lines) and

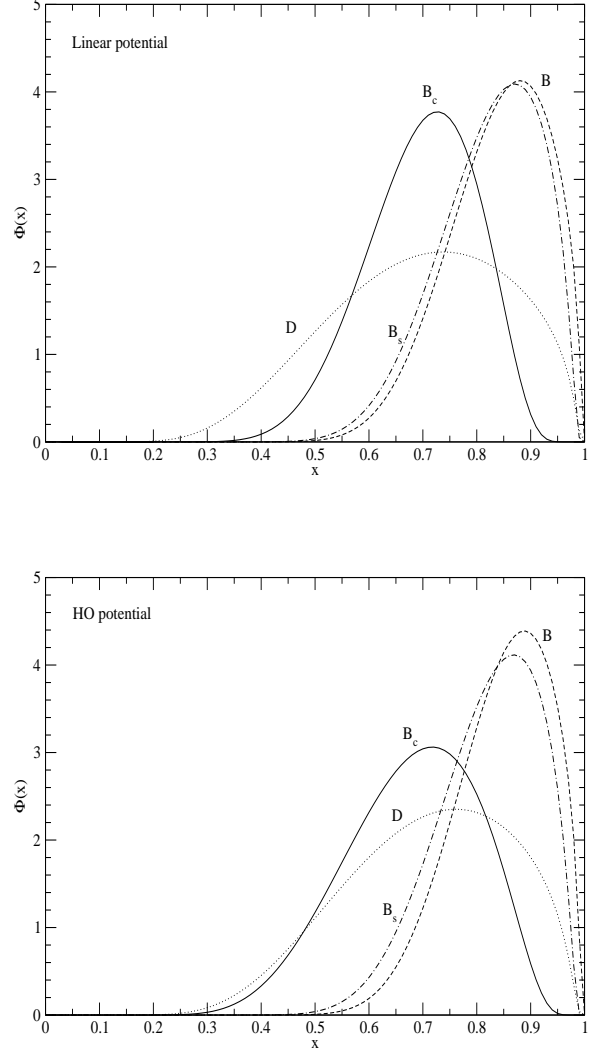


FIG. 2: The normalized distribution amplitudes for D , B , B_s , and B_c mesons obtained from the linear (upper panel) and HO (lower panel) potential parameters.

HO (dashed lines) potential parameters. While the two model predictions for the heavy-light systems such as $(D, B, \text{ and } B_s)$ are not much different from each other, the HO potential model predictions for the heavy-heavy systems such as $(\eta_c, B_c \text{ and } \eta_b)$ give somewhat broader shapes than the linear potential model predictions.

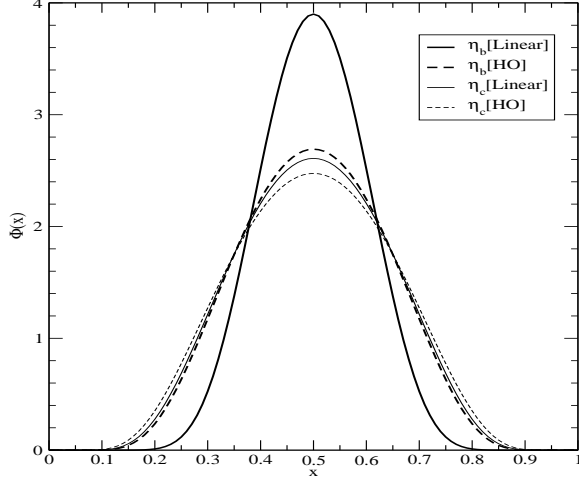


FIG. 3: The normalized distribution amplitudes for η_c (thin lines) and η_b (thick lines) mesons obtained from the linear (solid lines) and HO (dashed lines) potential parameters.

III. SEMILEPTONIC DECAYS OF THE B_c MESON

The amplitude A for a semileptonic decay of a meson $Q_1\bar{q}$ with the four-momentum P_1 and the mass M_1 into another meson $Q_2\bar{q}$ with the four-momentum P_2 and the mass M_2 is given by

$$A = \frac{G_F}{\sqrt{2}} V_{Q_1\bar{Q}_2} L_\mu H^\mu, \quad (12)$$

where G_F is the Fermi constant, $V_{Q_1\bar{Q}_2}$ is the relevant CKM mixing matrix element, L_μ is the lepton current

$$L_\mu = \bar{u}_{\nu_\ell} \gamma_\mu (1 - \gamma^5) v_\ell, \quad (13)$$

and H^μ is the hadron current

$$H^\mu = \langle P_2, \epsilon | (V^\mu - A^\mu) | P_1 \rangle. \quad (14)$$

Here, ϵ is the polarization of the daughter meson and V^μ and A^μ are the vector and axial vector currents, respectively. If the final state is pseudoscalar, the hadron current can be decomposed as follows:

$$\begin{aligned} \langle P_2 | A^\mu | P_1 \rangle &= 0, \\ \langle P_2 | V^\mu | P_1 \rangle &= f_+(q^2)(P_1 + P_2)^\mu + f_-(q^2)q^\mu, \end{aligned} \quad (15)$$

where $q^\mu = (P_1 - P_2)^\mu$ is the four-momentum transfer to the lepton pair ($\ell\nu_\ell$) and $m_\ell^2 \leq q^2 \leq (M_1 - M_2)^2$. Sometimes it is useful to express the matrix element of the vector current in terms of $f_+(q^2)$ and $f_0(q^2)$, which correspond to the transition amplitudes with 1^- and 0^+ spin-parity quantum numbers in the center of mass of the lepton pair, respectively. They satisfy the following

relation:

$$f_0(q^2) = f_+(q^2) + \frac{q^2}{M_1^2 - M_2^2} f_-(q^2). \quad (16)$$

Including the nonzero lepton mass, the differential decay rate for the exclusive $0^- \rightarrow 0^- \ell \nu_\ell$ process is given by [38]

$$\begin{aligned} \frac{d\Gamma}{dq^2} &= \frac{G_F^2}{24\pi^3} |V_{Q_1\bar{Q}_2}|^2 K(q^2) \left(1 - \frac{m_\ell^2}{q^2}\right)^2 \\ &\times \left\{ [K(q^2)]^2 \left(1 + \frac{m_\ell^2}{2q^2}\right) |f_+(q^2)|^2 \right. \\ &\left. + M_1^2 \left(1 - \frac{M_2^2}{M_1^2}\right)^2 \frac{3}{8} \frac{m_\ell^2}{q^2} |f_0(q^2)|^2 \right\}, \end{aligned} \quad (17)$$

where $K(q^2)$ is the kinematic factor given by

$$K(q^2) = \frac{1}{2M_1} \sqrt{(M_1^2 + M_2^2 - q^2)^2 - 4M_1^2 M_2^2}. \quad (18)$$

As we have discussed in Refs. [26, 27], the form factor $f_+(q^2)$ can be obtained just from the valence contribution in the $q^+ = 0$ frame with the “+” component of the currents without encountering the zero-mode contribution [39]. Thus, we perform our LFQM calculation in the $q^+ = 0$ frame, where $q^2 = q^+ q^- - \mathbf{q}_\perp^2 = -\mathbf{q}_\perp^2 < 0$, and then analytically continue the form factor $f_+(\mathbf{q}_\perp^2)$ in the spacelike region to the timelike region by changing \mathbf{q}_\perp^2 to $-q^2$ in the form factor. However, the form factor $f_-(q^2)$ receives the higher Fock state contribution (i.e., the zero-mode in the $q^+ = 0$ frame or the nonvalence contribution in the $q^+ > 0$ frame) within the framework of LF quantization. Thus, it is necessary to include either the zero-mode contribution (if working in the $q^+ = 0$ frame) or the nonvalence contribution (if working in the $q^+ > 0$ frame) to obtain the form factor $f_-(q^2)$. In order to calculate the weak form factor $f_-(q^2)$, we developed in [26, 27] an effective treatment of handling the higher Fock state (or nonvalence) contribution to $f_-(q^2)$ in the purely longitudinal $q^+ > 0$ frame (i.e., $q^2 = q^+ q^- > 0$), based on the BS formalism. Our effective method of calculating nonvalence contributions has been checked by testing the covariance of the model. For example, the effective method can be applied to the calculation of $f_+(q^2)$ and compared to the result obtained by the analytic continuation as described above. As shown below in our numerical calculations (see, e.g., Fig 4), the two results (one from the analytic continuation and the other from the effective method) agree to each other very closely. With this reasoning, we utilize the effective method in the $q^+ > 0$ frame to obtain $f_-(q^2)$ while we use the analytic continuation method to obtain $f_+(q^2)$ in the $q^+ = 0$ frame. Since the detailed calculations of the two form factors were presented in Refs. [26, 27], we just list the final forms of the two form factors $f_+(q^2)$ and $f_-(q^2)$.

The form factor $f_+(q^2)$ obtained from the $q^+ = 0$ frame

is given by

$$f_+(q^2) = \int_0^1 dx \int \frac{d^2 \mathbf{k}_\perp}{16\pi^3} \phi_2(x, \mathbf{k}'_\perp) \phi_1(x, \mathbf{k}_\perp) \times \frac{\mathcal{A}_1 \mathcal{A}_2 + \mathbf{k}_\perp \cdot \mathbf{k}'_\perp}{\sqrt{\mathcal{A}_1^2 + \mathbf{k}_\perp^2} \sqrt{\mathcal{A}_2^2 + \mathbf{k}'_\perp^2}}, \quad (19)$$

where $\mathbf{k}'_\perp = \mathbf{k}_\perp - (1-x)\mathbf{q}_\perp$ and $\mathcal{A}_i = m_i x + m_{\bar{q}}(1-x)$ ($i = 1, 2$).

The form factors $f_\pm(q^2)$ obtained from the purely longitudinal $q^+ > 0$ frame are given by [27]

$$f_\pm(q^2) = \pm \frac{(1 \mp \alpha_-)j^+(\alpha_+) - (1 \mp \alpha_+)j^+(\alpha_-)}{\alpha_+ - \alpha_-}, \quad (20)$$

where $\alpha = P_2^+/P_1^+$ is the momentum fraction satisfying $q^2 = (1-\alpha)(M_1^2 - M_2^2/\alpha)$ and

$$\alpha_\pm = \frac{M_2}{M_1} \left[\frac{M_1^2 + M_2^2 - q^2}{2M_1 M_2} \pm \sqrt{\left(\frac{M_1^2 + M_2^2 - q^2}{2M_1 M_2} \right)^2 - 1} \right]. \quad (21)$$

The $+$ ($-$) sign in Eq. (21) corresponds to the daughter meson recoiling in the positive(negative) z direction relative to the parent meson. The matrix element of the current j^+ is represented by the sum of the particle-number-conserving (valence) Fock state contribution, j_{val}^+ , and the particle-number-nonconserving (nonvalence) Fock state contribution, j_{nv}^+ . The matrix element of j_{val}^+ is given by [27]

$$j_{val}^+ = \int_0^\alpha dx \int \frac{d^2 \mathbf{k}_\perp}{16\pi^3} \phi_2(x', \mathbf{k}_\perp) \phi_1(x, \mathbf{k}_\perp) \times \frac{\mathcal{B}_1 \mathcal{B}_2 + \mathbf{k}_\perp^2}{\sqrt{\mathcal{B}_1^2 + \mathbf{k}_\perp^2} \sqrt{\mathcal{B}_2^2 + \mathbf{k}_\perp^2}}, \quad (22)$$

where $x' = x/\alpha$, $\mathcal{B}_1 = m_1 x + m_{\bar{q}}(1-x)$ and $\mathcal{B}_2 = m_2 x' + m_{\bar{q}}(1-x')$. The matrix element of j_{nv}^+ is obtained as [27]

$$j_{nv}^+ = \int_\alpha^1 \frac{dx}{x'(1-x')} \int \frac{d^2 \mathbf{k}_\perp}{16\pi^3} \chi^g(x, \mathbf{k}_\perp) \phi_1(x, \mathbf{k}_\perp) \times \frac{\mathbf{k}_\perp^2 + \mathcal{B}_1 \mathcal{B}_2 + x(1-x)(1-x')(M_1^2 - M_0^2)}{\sqrt{x(1-x)} \tilde{M}_0} \times G(x, \mathbf{k}_\perp), \quad (23)$$

where the LF vertex function of a gauge boson is given by

$$\chi^g(x, \mathbf{k}_\perp) = \frac{1}{\alpha \left[\frac{q^2}{1-\alpha} - \left(\frac{\mathbf{k}_\perp^2 + m_1^2}{1-x} + \frac{\mathbf{k}_\perp^2 + m_2^2}{x-\alpha} \right) \right]}, \quad (24)$$

and the final state meson-quark vertex is summarized in

$$G(x, \mathbf{k}_\perp) \propto \int dy \int d^2 \mathbf{l}_\perp \mathcal{K}(x, \mathbf{k}_\perp; y, \mathbf{l}_\perp) \phi_2(y, \mathbf{l}_\perp), \quad (25)$$

with \mathcal{K} being the BS kernel at the final state meson-quark vertex which in principle includes all the higher

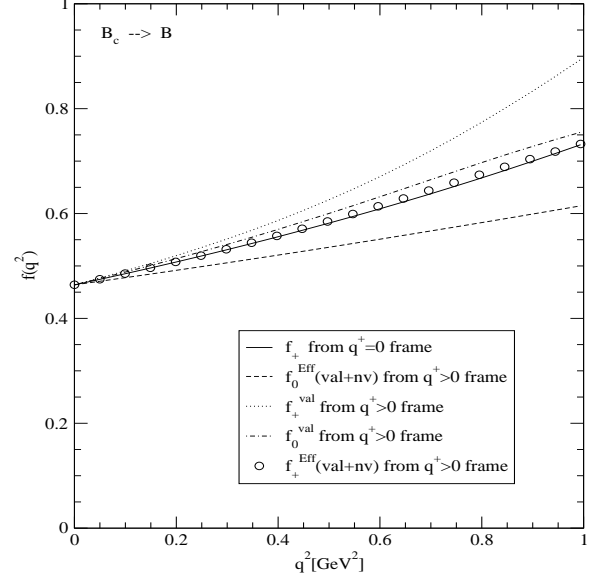


FIG. 4: The weak form factors for $B_c \rightarrow B$ semileptonic decays obtained from the $q^+ = 0$ and $q^+ > 0$ frames using the linear potential model.

Fock state contributions. In this work, we use the mean value theorem to approximate $G(x, \mathbf{k}_\perp)$ as a constant which has been tested in our previous works [26, 27, 40] and verified to be a good approximation.

In Fig. 4, we show our results of the weak form factors for the semileptonic $B_c \rightarrow B$ decay obtained from the linear potential model. The solid line represents our analytic($q^+ = 0$ frame) solution of $f_+(q^2)$, which is immune to the zero-mode contribution. The dotted and dot-dashed lines represent the weak form factors $f_+(q^2)$ and $f_0(q^2)$ obtained from the valence contributions in the purely longitudinal $q^+ > 0$ frame. The circled symbol denotes our effective ($q^+ > 0$ frame) solution of $f_+(q^2)$ including both valence and nonvalence contributions with a constant $G_{B_c B} = 15.0$ fixed by the normalization of $f_+(q^2)$ in the $q^+ = 0$ frame (solid line) at the $q^2 = 0$ limit. The dashed line represents our effective solution of $f_0(q^2)$ including both valence and nonvalence contributions with the same constant mean value $G_{B_c B} = 15.0$.

There are a few points to mention for this semileptonic $B_c \rightarrow B$ decay: (1) The weak form factor $f_+(q^2)$ (solid line) obtained from the $q^+ = 0$ frame is the exact solution since it is immune to the zero-mode contribution. (2) The valence contribution to $f_+(q^2)$ (dotted line) in the $q^+ > 0$ frame is exact only at the maximum recoil point (i.e., $q^2 = 0$) and the difference between the solid and dotted lines represents the nonvalence contribution to $f_+(q^2)$ in the $q^+ > 0$ frame, which is quite substantial near the zero recoil point (i.e., $q^2 = q_{\text{max}}^2$). (3) Our effective solution for f_+ (circle) including both valence and nonvalence contributions in the $q^+ > 0$ frame is very close to the analytic solution (solid line) for the entire

kinematic region. This justifies the reliability of our effective method as well as the mean value approximation to take the constant $G_{B_c B}$ for $G(x, \mathbf{k}_\perp)$. (4) Using the same constant $G_{B_c B} = 15.0$, we then obtain the effective solution of the $f_0(q^2)$ (dashed line) in the $q^+ > 0$ frame. Accordingly, the difference between our effective solution (dashed line) of $f_0(q^2)$ and the valence contribution (dot-dashed line) to $f_0(q^2)$ represents the nonvalence contribution to $f_0(q^2)$ in the $q^+ > 0$ frame.

In Sec. V, we will present our numerical calculations of the B_c semileptonic decays to other mesons and show the weak form factors $f_+(q^2)$ (solid line) obtained from our analytic method in the $q^+ = 0$ frame and $f_0(q^2)$ (dashed line) obtained from our effective method in $q^+ > 0$ frame.

IV. RADIATIVE $B_c^* \rightarrow B_c \gamma$ DECAY

In addition to semileptonic decays, the radiative decays of vector mesons can be analyzed within our LFQM [24, 28]. In this work, we thus calculate the decay rates for $B_c^* \rightarrow B_c \gamma$ transition.

In our LFQM calculation of $B_c^* \rightarrow B_c \gamma$ process, we first analyze the virtual photon (γ^*) decay process, calculating the momentum dependent transition form factor, $F_{B_c^* B_c}(q^2)$. The transition form factor $F_{B_c^* B_c}(q^2)$ for $B_c^*(P_1) \rightarrow B_c(P_2) + \gamma^*(q)$ is defined as [28]

$$\langle P_2 | V^\mu | P_1, h \rangle = i e \epsilon^{\mu\nu\rho\sigma} \epsilon_\nu(P_1, h) q_\rho P_{1\sigma} F_{B_c^* B_c}(q^2), \quad (26)$$

where the antisymmetric tensor $\epsilon^{\mu\nu\rho\sigma}$ assures electromagnetic gauge invariance, $q = P_1 - P_2$ is the four-momentum of the virtual photon, $\epsilon_\nu(P_1, h)$ is the polarization vector of the initial meson with the four-momentum P_1 and the helicity h . The kinematically allowed q^2 (momentum transfer squared) ranges from 0 to $q_{\text{max}}^2 = (M_{B_c^*} - M_{B_c})^2$. The decay form factor $F_{B_c^* B_c}(q^2)$ can also be obtained in the $q^+ = 0$ frame with the transverse ($h = \pm 1$) polarization and the “+”-component of currents without encountering zero-mode contributions [39] and then analytically continued from the spacelike region where the form factor is given by $F_{B_c^* B_c}(\mathbf{q}_\perp^2)$ to the timelike $q^2 > 0$ region by changing \mathbf{q}_\perp^2 to $-q^2$ in the form factor.

The decay form factor $F_{B_c^* B_c}(q^2)$ is then obtained as [28]

$$F_{B_c^* B_c}(q^2) = e_1 I(m_1, m_2, q^2) + e_2 I(m_2, m_1, q^2), \quad (27)$$

where the one loop integral $I(m_1, m_2, q^2)$ is given by

$$I(m_1, m_2, q^2) = \int_0^1 \frac{dx}{8\pi^3} \int d^2 \mathbf{k}_\perp \frac{\phi(x, \mathbf{k}'_\perp) \phi(x, \mathbf{k}_\perp)}{x_1 \tilde{M}_0 \tilde{M}'_0} \times \left\{ \mathcal{A} + \frac{2}{\mathcal{M}_0} [\mathbf{k}_\perp^2 - \frac{(\mathbf{k}_\perp \cdot \mathbf{q}_\perp)^2}{\mathbf{q}_\perp^2}] \right\}. \quad (28)$$

The primed factors in Eq. (28) are the functions of the final state momenta, e.g., $\tilde{M}'_0 = \tilde{M}'_0(x, \mathbf{k}'_\perp)$. The coupling

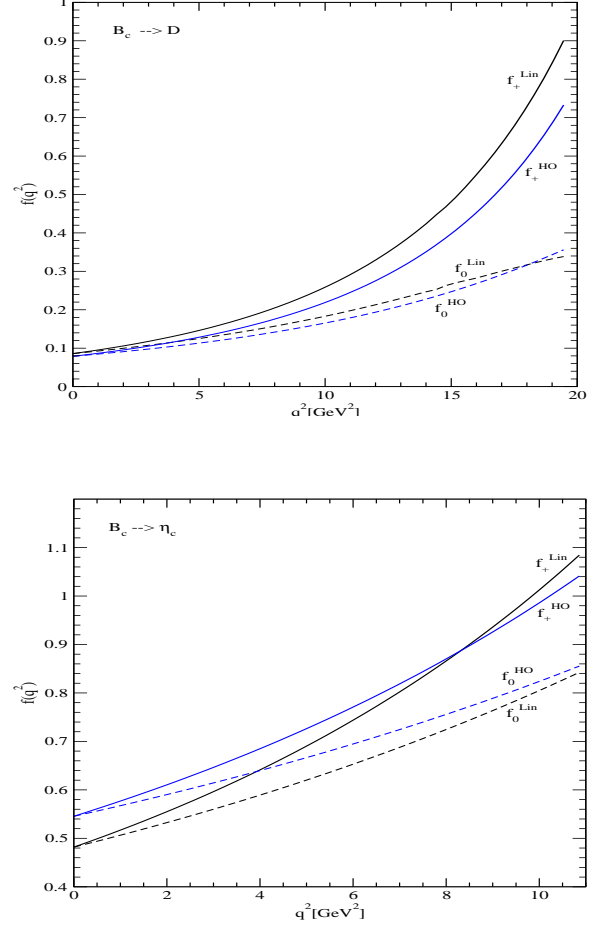


FIG. 5: (color online). The weak form factors $f_+(q^2)$ (solid line) and $f_0(q^2)$ (dashed line) for $B_c \rightarrow D$ (upper panel) and $B_c \rightarrow \eta_c$ (lower panel) semileptonic decays obtained from the linear (black line) and HO (blue line) potential parameters.

constant $g_{B_c^* B_c \gamma}$ for real photon (γ) case can then be determined in the limit $q^2 \rightarrow 0$, i.e., $g_{B_c^* B_c \gamma} = F_{B_c^* B_c}(q^2 = 0)$. The decay width for $V \rightarrow P \gamma$ is given by

$$\Gamma(B_c^* \rightarrow B_c \gamma) = \frac{\alpha}{3} g_{B_c^* B_c \gamma}^2 k_\gamma^3, \quad (29)$$

where α is the fine-structure constant and $k_\gamma = (M_{B_c^*}^2 - M_{B_c}^2)/2M_{B_c^*}$ is the kinematically allowed energy of the outgoing photon.

V. NUMERICAL RESULTS

In our numerical calculations of exclusive B_c decays, we use two sets of model parameters (m, β) for the linear and HO confining potentials given in Table I obtained from the calculation of the mass spectra. Although our predictions of ground state heavy meson masses are overall in good agreement with the experimental values, we

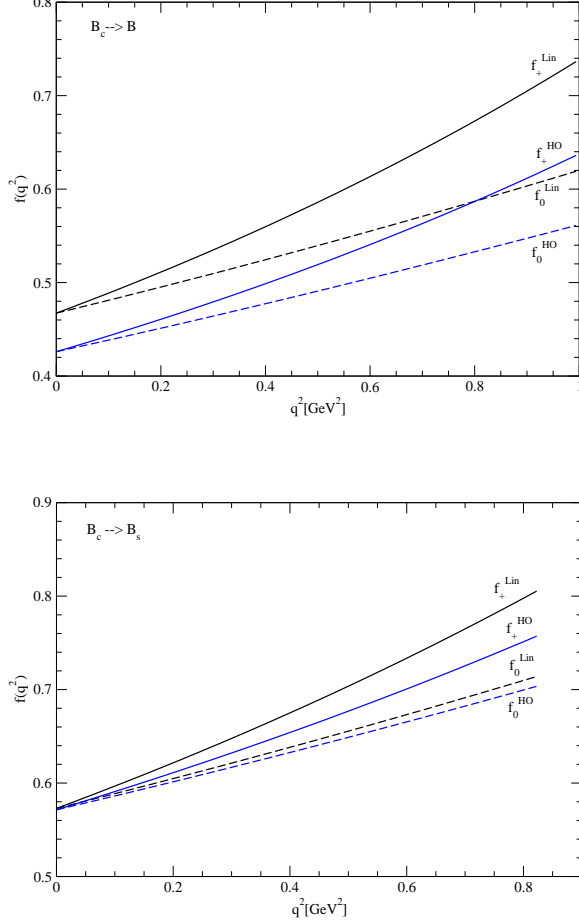


FIG. 6: (color online). The weak form factors $f_+(q^2)$ and $f_0(q^2)$ for $B_c \rightarrow B$ (upper panel) and $B_c \rightarrow B_s$ (lower panel) semileptonic decays obtained from the linear and HO potential parameters. The same line codes are used as in Fig. 5.

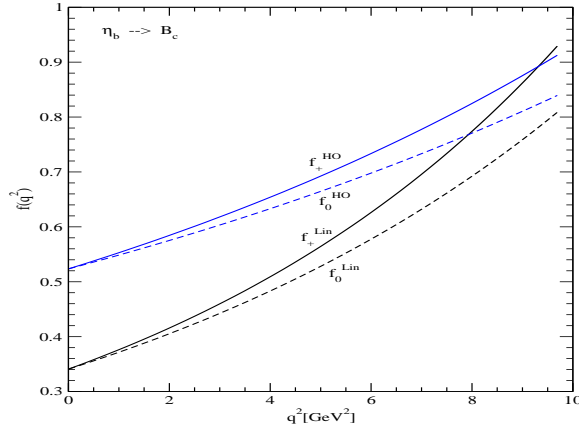


FIG. 7: (color online). The weak form factors $f_+(q^2)$ and $f_0(q^2)$ for $\eta_b \rightarrow B_c$ semileptonic decay obtained from the linear and HO potential parameters. The same line codes are used as in Fig. 5.

use the experimental meson masses [32] in the computations of the decay widths to reduce possible theoretical uncertainties. We also use the central values of the CKM matrix elements,

$$\begin{aligned} |V_{ub}| &= 0.00393, & |V_{cb}| &= 0.0412, \\ |V_{cd}| &= 0.230, & |V_{cs}| &= 1.04, \end{aligned} \quad (30)$$

quoted by the Particle Data Group (PDG) [32].

In Figs. 5 and 6 we show the q^2 -dependence of the weak form factors $f_+(q^2)$ and $f_0(q^2)$ in the whole kinematical range for the CKM-suppressed (enhanced) semileptonic $B_c \rightarrow D(\eta_c)$ (Fig. 5) and $B_c \rightarrow B(B_s)$ (Fig. 6) decays obtained from the linear and HO potentials. The line codes are explained in each figure. The used constant mean values for the calculations of the form factors $f_0(q^2)$ are $G_{B_c D} = 16.0$ [8.0], $G_{B_c \eta_c} = 11.0$ [5.0], $G_{B_c B} = 15.0$ [10.0] and $G_{B_c B_s} = 12.0$ [8.0] for the linear [HO] potential model. The form factor $f_+(q^2)$ (Eq. (19)) is obtained from our analytic method in the $q^+ = 0$ frame with the “+”-component of the currents, which is free from the zero-mode contributions. However, the form factor $f_-(q^2)$ (Eq. (20)) is obtained from our effective method in the purely longitudinal $q^+ > 0$ frame. Thus, our result for the form factor $f_0(q^2)$ is the solution obtained by combining the analytic solution for the $f_+(q^2)$ and the effective solution for the $f_-(q^2)$.

The kinematical range for $B_c \rightarrow D(\eta_c)$ decays induced by $b \rightarrow u(c)$ transitions with the c quark being a spectator is considerably broader than that for $B_c \rightarrow B(B_s)$ decays induced by $c \rightarrow d(s)$ transitions with the b quark being a spectator. The form factors $f_+(q^2)$ and $f_0(q^2)$ at the zero-recoil point (i.e., $q^2 = q_{\text{max}}^2$) correspond to the overlap integral of the initial and final state meson wave functions. The maximum-recoil point (i.e., $q^2 = 0$) corresponds to a final state meson recoiling with the maximum three-momentum $|\vec{P}_f| = (M_{B_c}^2 - M_f^2)/2M_{B_c}$ in the rest frame of the B_c meson. Especially for the $B_c \rightarrow D$ decay, the light \bar{u} quark in D meson will typically recoil with the momentum comparable to or larger than the c quark mass due to the large recoil effect for $B_c \rightarrow D$ decay. In order for the final D meson to be bound, there must be a correspondingly large momentum transfer to the spectator c quark. Thus, the overlap between the initial and final meson wave functions at the maximum-recoil point is limited and yields smaller value of $f_+(0)$ for $B_c \rightarrow D$ decay than that for other processes. We also note that one cannot apply the heavy quark symmetry to the system with the two heavy quarks, due to the flavor symmetry breaking by the kinetic energy terms as discussed in [41].

Although there already exist various model predictions on the above B_c semileptonic decays, the predictions of the semileptonic $\eta_b \rightarrow B_c$ decay is not reported yet as far as we know. We thus show in Fig. 7 the q^2 -dependence of the weak form factors $f_+(q^2)$ and $f_0(q^2)$ for the semileptonic $\eta_b \rightarrow B_c$ decay obtained from the linear and HO potentials. The used constant mean value for the calculation of the form factor $f_0(q^2)$ is $G_{\eta_b B_c} = 13.0$ [4.0]

for the linear [HO] potential model. The same line codes presented in Fig. 5 are used in Fig. 7. While the linear and HO potential models give similar decay constants for heavy-light mesons (D, B, B_s) and η_c meson [28], they predict quite different values of B_c and η_b , e.g., $f_{\eta_b} = 507$ MeV and 897 MeV for the linear and HO potential models [28], respectively. This results in sizable differences between the two models for the prediction of the weak form factors $f_+(q^2)$ and $f_0(q^2)$ in the $\eta_b \rightarrow B_c$ decay. Since the linear potential model prediction of the quark DA for η_b is narrower than the HO model prediction (see Fig. 3), the overlap between the initial and final meson wave functions at the maximum-recoil point (i.e., $q^2 = 0$) produces smaller values of $f_+(=f_0)$ for the linear potential model than for the HO potential model. As shown in Fig. 1, our analysis of the η_b mass spectrum indicates that the very recent experimental data from the Babar experiment, $M_{\eta_b}^{\text{exp}} = 9388.8^{+3.1}_{-2.3} \pm 2.7$ MeV [33], may prefer the HO potential model prediction (9295 MeV) to the linear one (9657 MeV). We may thus expect that the weak form factors for $\eta_b \rightarrow B_c$, if measured, would be closer to the HO potential model prediction than for the linear one.

In Figs. 8-10, we show the differential decay widths $d\Gamma/dq^2$ for the $B_c \rightarrow D(\eta_c)\ell\nu_\ell$ (Fig. 8), $B_c \rightarrow B(B_s)\ell\nu_\ell$ (Fig. 9) and $\eta_b \rightarrow B_c\ell\nu_\ell$ (Fig. 10) processes obtained from the linear and HO potential parameters. The line codes are described in each figure. We should note that the minimum q^2 value of the form factor depends on the actual final lepton and it is given (neglecting neutrino masses) by the lepton mass as $q_{\text{min}}^2 = m_\ell^2$. Although the difference between the linear and HO model predictions are not very large for the $B_c \rightarrow (B, B_s)$ processes, they are quite different for other processes, especially for the $\eta_b \rightarrow B_c$ process. Since the constituent masses of b - and c quarks are common to linear and HO model predictions, the difference of the decay rates for the $\eta_b \rightarrow B_c$ process seems to come from the different choice of the variational β parameters. We note, however, that the difference of the decay rates between the two models are significantly reduced for the heavy τ lepton case.

In Table III, we summarize our results for the weak form factors f_+ and f_0 at $q^2 = 0$ and q_{max}^2 and the decay widths Γ_ℓ of the semileptonic $B_c \rightarrow (D, \eta_c, B, B_s)\ell\nu_\ell$ and $\eta_b \rightarrow B_c\ell\nu_\ell$ ($\ell = e, \mu, \tau$) decays in comparison with other theoretical model predictions [5, 9, 10, 13, 14, 15, 16, 17, 42]. The subscript for the decay width Γ_ℓ represents the result for $P \rightarrow P\ell\nu_\ell$ decay where the final lepton is $\ell = e, \mu$ or τ . For the decays induced by $b \rightarrow u(c)$ transitions such as $B_c \rightarrow D, \eta_c$ and $\eta_b \rightarrow B_c$ decays, we take $\Gamma_e \simeq \Gamma_\mu$ with the massless lepton limit since the muon mass effect is negligible for these transitions with large kinematic ranges. For the decays induced by $c \rightarrow d(s)$ transitions such as $B_c \rightarrow B(B_s)$ decays, Γ_μ is about 5% smaller than Γ_e in our model predictions. For the $B_c \rightarrow D$ decay, our predictions of the form factor f_+ at the maximum-recoil point are rather smaller than other quark model predictions. The upcoming experi-

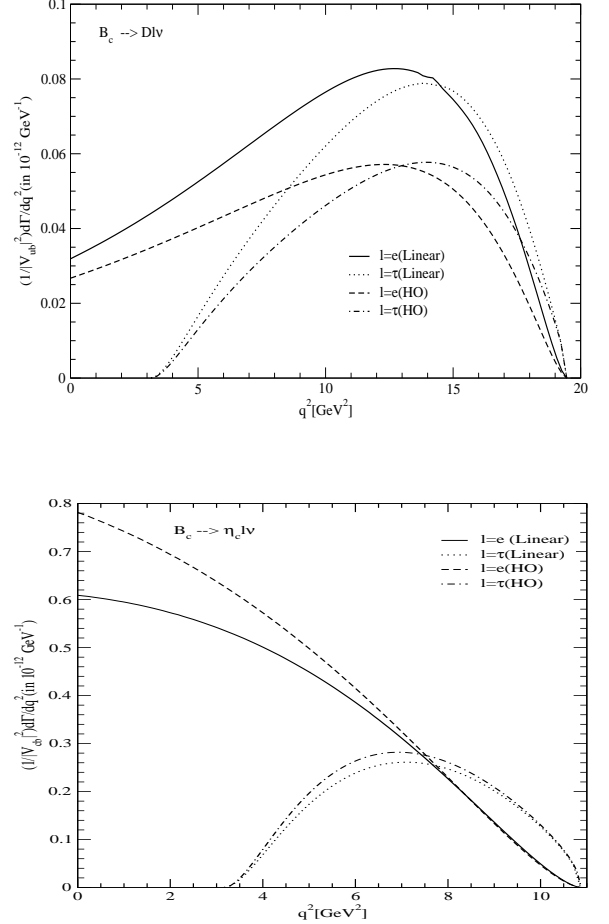


FIG. 8: Differential decay widths $(1/|V_{Q_1 Q_2}|^2)d\Gamma/dq^2$ (in units of $10^{-12} \text{ GeV}^{-1}$) for $B_c \rightarrow D\ell\nu_\ell$ and $B_c \rightarrow \eta_c\ell\nu_\ell$ processes obtained from the linear and HO potential parameters.

mental study planned at the Tevatron and at the LHC may distinguish these different model predictions. For the $B_c \rightarrow \eta_c, B$ and B_s semileptonic decays, our predictions are quite comparable with those of the quasipotential approach to the relativistic quark model [9, 10], the relativistic quark-meson model [15], and the nonrelativistic quark model [16]. It may be noted, however, that the predictions of the quark model based on an effective Lagrangian describing the coupling of hadrons to their constituent quarks [5] as well as the covariant LFQM [17] are quite different from other model predictions including ours.

We should also note that the decay rates Γ_e obtained from the valence contributions to $f_+(q^2)$ in the $q^+ > 0$ frame compared to the analytic solutions $f_+(q^2)$ in the $q^+ = 0$ frame are estimated about (70 ~ 100)% for the processes considered in this work. This indicates that the huge nonvalence contributions to $f_+(q^2)$ in the $q^+ > 0$ frame are needed for restoring covariance of the model. On the other hand, the decay rates Γ_e obtained from our

TABLE III: Form factors f_+ and f_0 evaluated at $q^2 = 0$ and q_{\max}^2 and decay widths Γ_ℓ (in 10^{-15} GeV) for $B_c \rightarrow (D, \eta_c, B, B_s)\ell\nu_\ell$ and $\eta_b \rightarrow B_c\ell\nu_\ell$ ($\ell = e, \mu, \tau$) transitions.

Mode	Linear[HO]	EFG [9, 10]	IKS [5]	NW [15]	HNv [16]	AKN [42]	CD [14]	WSL [17]	
$B_c \rightarrow D$	$f_{+(0)}(0)$	0.086[0.079]	0.14	0.69	0.1446	-	0.089	-	0.16
	$f_{+}(q_{\max}^2)$	0.901[0.733]	1.20	2.20	1.017	-	-	0.59	1.10
	$f_0(q_{\max}^2)$	0.338[0.345]	0.64	-	-	-	-	-	0.59
	$\Gamma_{e(\mu)}$	0.017[0.013]	0.019	0.26	0.020	-	-	0.005(0.03)	0.043
	Γ_τ	(0.012 \pm 0.003)[0.0094 \pm 0.0023]	-	-	-	-	-	-	-
$B_c \rightarrow \eta_c$	$f_{+(0)}(0)$	0.482[0.546]	0.47	0.76	0.5359	0.49	0.622	-	0.61
	$f_{+}(q_{\max}^2)$	1.084[1.041]	1.07	1.07	1.034	1.00	-	0.94	1.10
	$f_0(q_{\max}^2)$	0.842[0.855]	0.92	-	-	0.91	-	-	0.86
	$\Gamma_{e(\mu)}$	6.91[7.95]	5.9	14.0	6.8	6.95	8.6	2.1(6.9)	9.81
	Γ_τ	(2.25 \pm 0.45)[2.43 \pm 0.49]	-	3.52	-	2.46	3.3 \pm 0.9	-	-
$B_c \rightarrow B$	$f_{+(0)}(0)$	0.467[0.426]	0.39	0.58	0.4504	0.39	0.362	-	0.63
	$f_{+}(q_{\max}^2)$	0.736[0.636]	0.96	0.96	0.6816	0.70	-	0.66	0.97
	$f_0(q_{\max}^2)$	0.619[0.561]	0.80	-	-	0.71	-	-	0.81
	Γ_e	0.85[0.68]	0.6	2.1	0.638	0.65	-	0.9(1.0)	1.63
	Γ_μ	(0.81 \pm 0.02)[0.65 \pm 0.02]	-	-	-	0.63	-	-	-
$B_c \rightarrow B_s$	$f_{+(0)}(0)$	0.573[0.571]	0.50	0.61	0.5917	0.58	0.564	-	0.73
	$f_{+}(q_{\max}^2)$	0.805[0.757]	0.99	0.92	0.8075	0.86	-	0.66	1.03
	$f_0(q_{\max}^2)$	0.714[0.704]	0.86	-	-	0.86	-	-	0.87
	Γ_e	15.55[14.90]	12	29	12.35	15.1	15	11.1(12.9)	23.45
	Γ_μ	(14.69 \pm 0.29)[14.07 \pm 0.28]	-	-	-	14.5	-	-	-
$\eta_b \rightarrow B_c$	$f_{+(0)}(0)$	0.341[0.523]	-	-	-	-	-	-	-
	$f_{+}(q_{\max}^2)$	0.929[0.913]	-	-	-	-	-	-	-
	$f_0(q_{\max}^2)$	0.809[0.839]	-	-	-	-	-	-	-
	$\Gamma_{e(\mu)}$	4.60[7.93]	-	-	-	-	-	-	-
	Γ_τ	(1.57 \pm 0.31)[2.11 \pm 0.42]	-	-	-	-	-	-	-

effective solutions $f_+(q^2)$ in the $q^+ > 0$ frame compared to the analytic solutions $f_+(q^2)$ in the $q^+ = 0$ frame are estimated about (20 \sim 25)% differences for the processes with large kinematic regions such as $B_c \rightarrow D(\eta_c)e\nu_e$ and $\eta_b \rightarrow B_c e\nu_e$ decays and about (1 \sim 3)% differences for those with small kinematic regions such as $B_c \rightarrow B e\nu_e$ and $B_c \rightarrow B_s e\nu_e$ decays. Those error estimates do not affect our predictions for the decay rates with the massless electron where only $f_+(q^2)$ is used. However, they may affect our predictions for the decay rates with the (μ, τ) leptons and thus we included them in Table III. Our effective solutions obviously reduce the difference a lot between the valence contribution to $f_+(q^2)$ in the $q^+ > 0$ frame and the analytic solution to $f_+(q^2)$ in the $q^+ = 0$ frame but still needs to be improved for the processes with large kinematic regions.

Finally, in order to analyze the total rate for the radiative $B_c^* \rightarrow B_c + \gamma$ decay, the masses of the B_c and B_c^* mesons must be specified. Although we predicted the above two meson masses in Fig. 1, we use the the central value of the experimental data $M_{B_c^*}^{\text{exp}} = 6.276$ GeV [32] to reduce the possible theoretical uncertainties. For the unmeasured B_c^* meson mass, we take some range of the B_c^* meson mass, i.e., $10 \text{ MeV} \leq \Delta m (= M_{B_c^*} - M_{B_c}) \leq 220 \text{ MeV}$. The upper value of Δm (i.e., $M_{B_c^*} = 6496 \text{ MeV}$) is chosen to be corresponding to our predictions, $M_{B_c^*} = 6494 \text{ MeV}$ and 6492 MeV , obtained from the linear and HO potential models, respectively.

In Fig. 11, we show the momentum-dependent form

factor $F_{B_c^* B_c}(q^2)$ (upper panel) for the radiative $B_c^* \rightarrow B_c \gamma^*$ decay and the dependence of $\Gamma(B_c^* \rightarrow B_c \gamma)$ on Δm (lower panel) obtained from the linear (solid line) and HO potential (dashed line) parameters. For the transition form factor $F_{B_c^* B_c}(q^2)$, we have performed the analytic continuation of $F_{B_c^* B_c}(q^2)$ from the spacelike region ($q^2 < 0$) to the physical timelike $0 \leq q^2 \leq q_{\max}^2$, where $q_{\max}^2 = (M_{B_c^*} - M_{B_c})^2$ represents the zero recoil point of the B_c meson. The coupling constant $g_{B_c^* B_c}$ is obtained at the $q^2 = 0$ point that corresponds to the B_c meson recoiling with the maximum three-momentum in the rest frame of the B_c^* meson. In our model calculation, the coupling constant itself is independent of the physical masses of the mesons and our prediction is $g_{B_c^* B_c} = 0.273$ [0.257] GeV^{-1} for the linear [HO] potential model. Our predictions are quite comparable with the result from the QCD sum rule approach [43], $g_{B_c^* B_c}^{SR} = 0.270 \pm 0.095 \text{ GeV}^{-1}$. As one can see from the lower panel of Fig. 11, the dependence of $\Gamma(B_c^* \rightarrow B_c \gamma)$ on Δm is quite sensitive to the mass of the B_c^* meson, e.g., our linear [HO] potential model predicts $\Gamma(B_c^* \rightarrow B_c \gamma) = 22.4$ [19.9] $\text{eV} \sim 1836$ [1631] eV for $\Delta m = 50 \text{ MeV} \sim 220 \text{ MeV}$. This sensitivity for the B_c^* radiative decay may help in determining the mass of B_c^* experimentally and pinning down the best phenomenological model. Other magnetic dipole decays $V \rightarrow P\gamma$ of various heavy-flavored mesons such as $(D, D^*, D_s, D_s^*, \eta_c, J/\psi)$ and $(B, B^*, B_s, B_s^*, \eta_b, \Upsilon)$ using our LFQM can be found in [28].

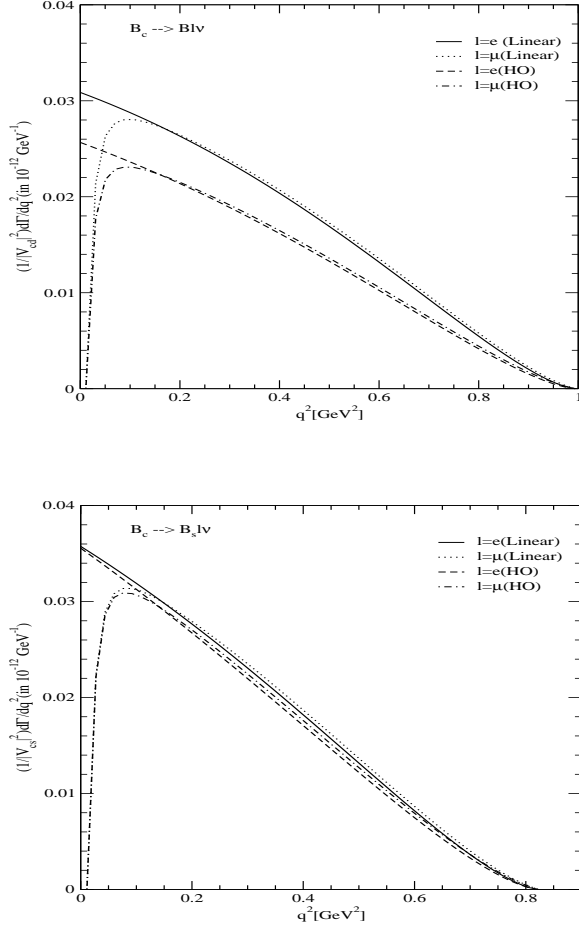


FIG. 9: Differential decay widths $(1/|V_{Q_1 Q_2}|^2)d\Gamma/dq^2$ (in units of $10^{-12} \text{ GeV}^{-1}$) for $B_c \rightarrow B\ell\nu_\ell$ and $B_c \rightarrow B_s\ell\nu_\ell$ processes obtained from the linear and HO potential parameters.

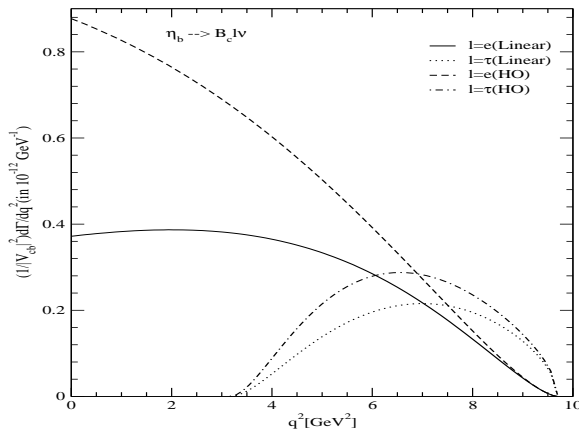


FIG. 10: Differential decay width $(1/|V_{Q_1 Q_2}|^2)d\Gamma/dq^2$ (in units of $10^{-12} \text{ GeV}^{-1}$) for $\eta_b \rightarrow B_c\ell\nu_\ell$ process obtained from the linear and HO potential parameters.

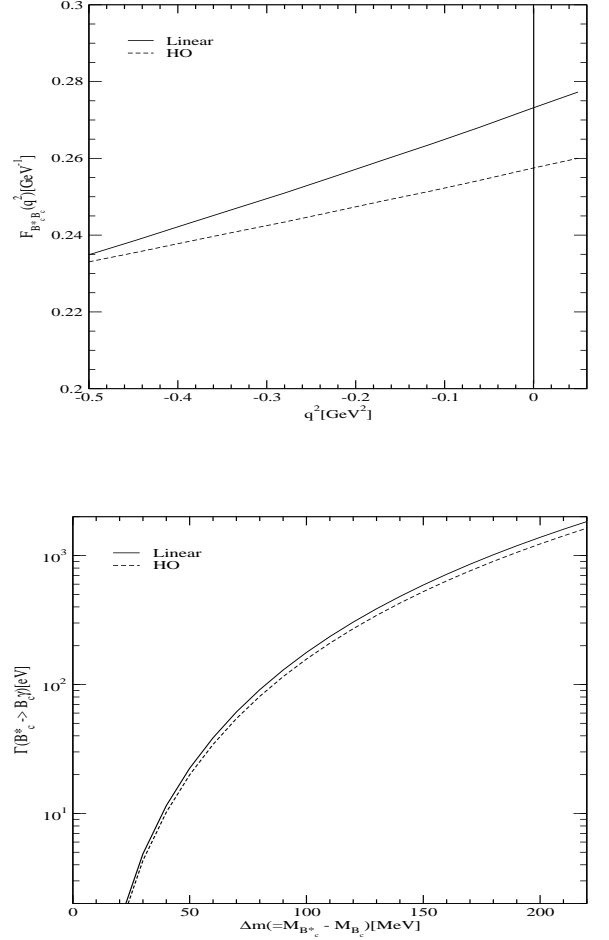


FIG. 11: The transition form factor $F_{B_c^* B_c}(q^2)$ (upper panel) for $B_c^* \rightarrow B_c\gamma^*$ and the dependence of $\Gamma(B_c^* \rightarrow B_c\gamma)$ (lower panel) on $\Delta m = M_{B_c^*} - M_{B_c}$ obtained from the linear and HO potential parameters, where the central value of the experimental data $M_{B_c}^{\text{exp}} = 6.276 \text{ GeV}$ [32] is used.

VI. SUMMARY AND DISCUSSION

In this work, we investigated the exclusive semileptonic $B_c \rightarrow (D, \eta_c, B, B_s)\ell\nu_\ell$, $\eta_b \rightarrow B_c\ell\nu_\ell$ ($\ell = e, \mu, \tau$) decays and the magnetic dipole $B_c^* \rightarrow B_c\gamma$ decay using our LFQM constrained by the variational principle for the QCD motivated effective Hamiltonian with the linear (or HO) plus Coulomb interaction. Especially, we obtained the new variational parameter β_{cb} for the bottom-charm sector and predicted the mass eigenvalues of the low-lying B_c and B_c^* states. Our new predictions of $M_{B_c} = 6459$ [6351] MeV obtained from the linear [HO] potential model is in agreement with the data, $M_{B_c}^{\text{exp}} = (6276 \pm 4) \text{ MeV}$ [32], within 3% error. We also predicted the unmeasured mass of B_c^* as $M_{B_c^*} = 6494$ [6496] MeV for the linear [HO] potential model. Our model parameters obtained from the variational principle uniquely determine

the physical quantities related to the above processes. This approach can establish the broader applicability of our LFQM to the wider range of hadronic phenomena. For instance, our LFQM has been tested extensively in the spacelike processes [24, 40] as well as in the timelike exclusive processes such as semileptonic [25, 26, 38] and rare [27] decays of pseudoscalar mesons and the magnetic dipole $V \rightarrow P\gamma^*$ decays [28, 29].

The weak form factor $f_+(q^2)$ for the semileptonic decays between two pseudoscalar mesons and the decay form factor $F_{B_c^* B_c}(q^2)$ for the $B_c^* \rightarrow B_c \gamma$ decay are obtained in the $q^+ = 0$ frame ($q^2 = -\mathbf{q}_\perp^2 < 0$) and then analytically continued to the timelike region by changing \mathbf{q}_\perp^2 to $-q^2$ in the form factor. The form factor $f_-(q^2)$ for the semileptonic decays between two pseudoscalar mesons is obtained from our effective treatment of the nonvalence contribution in addition to the valence one in the $q^+ > 0$ frame ($q^2 > 0$) based on the BS formalism. The covariance (i.e., frame independence) of our model has been checked by the comparison of $f_+(q^2)$ obtained in the $q^+ = 0$ frame with that obtained in the $q^+ > 0$ frame. Using the solutions of $f_+(q^2)$ obtained from the $q^+ = 0$ frame and $f_-(q^2)$ obtained from the $q^+ > 0$ frame, we calculated the decay rates for the ex-

clusive $B_c \rightarrow (D, \eta_c, B, B_s)\ell\nu_\ell$ and $\eta_b \rightarrow B_c \ell\nu_\ell$ decays and compared with other theoretical approaches. For the radiative $B_c^* \rightarrow B_c \gamma$ decay, we find that the decay width $\Gamma(B_c^* \rightarrow B_c \gamma)$ is very sensitive to the value of $\Delta m = M_{B_c^*} - M_{B_c}$. This sensitivity for the B_c^* radiative decay may help in determining the mass of B_c^* experimentally. Since the form factor $F_{B_c^* B_c}(q^2)$ for the radiative $B_c^* \rightarrow B_c \gamma$ decay presented in this work is analogous to the vector current form factor $g(q^2)$ in the weak decay of ground state vector meson to ground state pseudoscalar meson, the ability of our model in describing the radiative decay would therefore be relevant to the applicability of our model also for the weak decay. Consideration on such exclusive weak decays in our LFQM is underway.

Acknowledgments

The work of H.-M. Choi was supported by the Korea Research Foundation Grant funded by the Korean Government(KRF-2008-521-C00077) and that of C.-R. Ji by the U.S. Department of Energy(No. DE-FG02-03ER41260).

-
- [1] I. P. Gouz, V. V. Kiselev, A. K. Likhoded, V. I. Romanovsky, and O. P. Yushchenko, Phys. Atom. Nucl. **67**, 1559 (2004); Yad. Fiz. **67**, 1581 (2004).
 - [2] P. Colangelo, G. Nardulli, and N. Paver, Z. Phys. C **57**, 43 (1993).
 - [3] V. V. Kiselev, A. E. Kovalsky, and A. K. Likhoded, Nucl. Phys. B **585**, 353 (2000); V. V. Kiselev, A. K. Likhoded, and A. I. Onishchenko, Nucl. Phys. B **569**, 473 (2000).
 - [4] T. Huang and F. Zuo, Eur.Phys.J.C **51**, 833 (2007).
 - [5] M. A. Ivanov, J. G. Körner and P. Santorelli, Phys. Rev. D **63**, 074010 (2001).
 - [6] M. A. Ivanov, J. G. Körner and P. Santorelli, Phys. Rev. D **71**, 094006 (2005).
 - [7] M. A. Ivanov, J. G. Körner and P. Santorelli, Phys. Rev. D **73**, 054024 (2006).
 - [8] D. Ebert, R. N. Faustov and V. O. Galkin, Phys. Rev. D **67**, 014027 (2003).
 - [9] D. Ebert, R. N. Faustov and V. O. Galkin, Phys. Rev. D **68**, 094020 (2003).
 - [10] D. Ebert, R. N. Faustov and V. O. Galkin, Eur.Phys.J.C **32**, 29 (2003).
 - [11] C.-H. Chang and Y.-Q. Chen, Phys. Rev. D **49**, 3399 (1994).
 - [12] J.-F. Liu and K.-T. Chao, Phys. Rev. D **56**, 4133 (1997).
 - [13] A. Abd El-Hady, J. H. Munoz, and J. P. Vary, Phys. Rev. D **62**, 014019 (2000).
 - [14] P. Colangelo and F. De Fazio, Phys. Rev. D **61**, 034012 (2000).
 - [15] M. A. Nobes and R. M. Woloshyn, J. Phys. G **26**, 1079 (2000).
 - [16] E. Hernández, J. Nieves and J. M. Verde-Velasco, Phys. Rev. D **74**, 074008 (2006).
 - [17] W. Wang, Y.-L. Shen, and C.-D. Lü, arXiv:0811.3748[hep-ph].
 - [18] M. Lusignoli and M. Masetti, Z. Phys. C **51**, 549 (1991).
 - [19] D. Du and Z. Wang, Phys. Rev. D **39**, 1342 (1989).
 - [20] R. Dhir, N. Sharma, and R.C. Verma, J. Phys. G **35**, 085002 (2008).
 - [21] S. Godfrey, Phys. Rev. D **70**, 054017 (2004).
 - [22] M. Wirbel, B. Stech, and M. Bauer, Z. Phys. C **29**, 637 (1985); M. Bauer, B. Stech, and M. Wirbel, Z. Phys. C **34**, 103 (1987).
 - [23] N. Isgur, D. Scora, B. Grinstein, and M.B. Wise, Phys. Rev. D **39**, 799 (1989).
 - [24] H.-M. Choi and C.-R. Ji, Phys. Rev. D **59**, 074015 (1999).
 - [25] H.-M. Choi and C.-R. Ji, Phys. Lett. B **460**, 461 (1999).
 - [26] C.-R. Ji and H.-M. Choi, Phys. Lett. B **513**, 330 (2001).
 - [27] H.-M. Choi, C.-R. Ji, and L.S. Kisslinger, Phys. Rev. D **65**, 074032 (2002).
 - [28] H.-M. Choi, Phys. Rev. D **75**, 073016 (2007); J. Korean Phys. Soc. **53**, 1205 (2008).
 - [29] H.-M. Choi, Phys. Rev. D **77**, 097301 (2008).
 - [30] H.-M. Choi and C.-R. Ji, Phys. Rev. D **75**, 034019 (2007).
 - [31] D. Scora and N. Isgur, Phys. Rev. D **52**, 2783 (1995).
 - [32] C. Amsler *et al.* (Particle Data Group), Phys. Lett. B **667**, 1 (2008).
 - [33] P. Grenier, arXiv:0809.1672 [hep-ex].
 - [34] E. J. Eichten and C. Quigg, Phys. Rev. D **49**, 5845 (1994).
 - [35] S. S. Gershtein, V. V. Kiselev, A. K. Likhoded, and A.V. Tkabladze, Phys. Rev. D **51**, 3613 (1995).
 - [36] L. P. Fulcher, Phys. Rev. D **60**, 074006 (1999).
 - [37] S. Capstick and S. Godfrey, Phys. Rev. D **41**, 2856 (1990).
 - [38] H.-M. Choi and C.-R. Ji, Phys. Rev. D **59**, 034001 (1998).
 - [39] H.-M. Choi and C.-R. Ji, Phys. Rev. D **58**, 071901(R)

- (1998); Phys. Rev. D **72**, 013004 (2005); S. J. Brodsky and D. S. Hwang, Nucl. Phys. B **543**, 239 (1998).
- [40] H.-M. Choi, C.-R. Ji, and L.S. Kisslinger, Phys. Rev. D **64**, 093006 (2001); Phys. Rev. D **66**, 053011 (2002).
- [41] E. Jenkins, M. Luke, A. V. Manohar, and M. J. Savage, Nucl. Phys. B **390**, 463 (1993).
- [42] A.Yu. Anisimov, P. Yu. Kulikov, I.M. Narodetskii, and K.A. Ter-Martirosyan, Phys. Atom Nucl. **62**, 1739 (1999)[Yad. Fiz. **62**, 1868 (1999)].
- [43] T. M. Aliev, E. Iltan, and N. K. Pak, Phys. Lett. B **329**, 123 (1994).